ISSN 1063-7826, Semiconductors, 2008, Vol. 42, No. 5, pp. 616–623. © Pleiades Publishing, Ltd., 2008.
Original Russian Text © V.N. Jmerik, A.M. Mizerov, T.V. Shubina, D.S. Plotnikov, M.V. Zamoryanskaya, M.A. Yagovkina, Ya.V. Domracheva, A.A. Sitnikova, S.V. Ivanov, 2008, published in Fizika i Tekhnika Poluprovodnikov, 2008, Vol. 42, No. 5, pp. 630–638.

FABRICATION, TREATMENT, AND TESTING OF MATERIALS AND STRUCTURES

Features of the Spatial Distribution of Indium in InGaN Epitaxial Layers Grown by Plasma-Assisted Molecular Beam Epitaxy

V. N. Jmerik^, A. M. Mizerov, T. V. Shubina, D. S. Plotnikov, M. V. Zamoryanskaya, M. A. Yagovkina, Ya. V. Domracheva, A. A. Sitnikova, and S. V. Ivanov

Ioffe Physicotechnical Institute, Russian Academy of Sciences, Politekhnicheskaya ul. 26, St. Petersburg, 194021 Russia
^e-mail: jmerik@pls.ioffe.ru

Submitted September 25, 2007; accepted for publication October 17, 2007

Abstract—The processes leading to the formation of a spatially nonuniform distribution of indium in the $In_xGa_{1-x}N$ layers with $x = 0$–0.6 grown by molecular beam epitaxy with plasma activation of nitrogen at relatively low growth temperatures (590–630°C) are studied. It is found that at low values of $x < 0.1$, the growth proceeds pseudomorphically at least to a thickness of 70 nm, and these layers are characterized by a high uniformity of the In distribution, which confirms their thermodynamic stability. Upon increasing x up to ~0.3, the signs of a nonuniform In distribution are observed, which is associated with the stress relaxation facilitating the development of phase separation. It is shown that layers with In distribution of lower uniformity feature more intense photoluminescence in the energy range 2.0–2.5 eV. For the layers with $x \approx 0.6$, complete phase separation is observed with the formation of several phases with a wide range of compositions, including the region in the vicinity of the InN binary compound.

PACS numbers: 81.40.Tv, 81.05.Ee, 81.15.Gh

DOI: 10.1134/S1063782608050229

1. INTRODUCTION

In recent decades, the mass production of light-emitting and laser diodes based on wide-gap III–V compounds has become an important segment of the semiconductor industry. It is considered that a key role in the development of technologies of these devices was played by the unique properties of the $In_xGa_{1-x}N$/GaN heterostructures used in the active region of lasers. These properties are first of all associated with the existence of the localization effect of charge carriers in the InGaN compound, which emerges due to a spatially nonuniform In distribution in the layers (aggregation of In) with respect to the average In content (x) [1]. The development of the potential profile observed in this case restricts the lateral transport of nonequilibrium charge carriers, which leads to an increase in the efficiency of radiative recombination in device structures even at a relatively high density of grown-in dislocations (as high as ~10^9 cm^{-2}), which are the centers of nonradiative recombination.

Commercial III–N based light-emitting diodes (LEDs) are produced with a maximum working emission wavelength (λ_{max}) as high as 525 nm [2]. In the literature are reports on the fabrication of pilot samples of LEDs with $\lambda_{max} = 645$ nm. However, these devices had substantially smaller values of quantum efficiency and output optical power [3, 4]. For commercial laser diodes, the value of λ_{max} amounts to 440 nm, while for the best laboratory samples this value attains 485 nm [5]. Therefore, the represented values of λ_{max} for LEDs and laser diodes lie substantially lower than potentially possible and are in the infrared spectral region with $\lambda \approx$ 1800 nm for the III–N-based devices.

To expand the range of the effective operation of diodes into the long-wavelength spectral region ($\lambda >$ 525 nm), it is necessary to use $In_xGa_{1-x}N$ alloys with increased In content ($x > 0.20$). A substantial feature of these layers is the enhancement of the spatial nonuniformity of the In distribution with increasing x. This circumstance is conditioned by the development of a whole series of processes, among which, above all, it is necessary to notice a phenomenon of phase separation in InGaN alloys and processes of the surface and spatial segregation of In, accumulation of In at various defects (including dislocations, grain boundaries, and clusters of metal In), etc. Insufficient understanding and poor control over these processes led to the formation of a highly defect-containing cluster structure of InGaN alloys with a low efficiency of radiative recombination. Therefore, at the present time, not only attainment of materials with a specified value of x but also control over the spatial In distribution including the development of the methods for formation of coherent (defect-free) clusters of InGaN alloys with a controllable size and increased In content with respect to the matrix in a wide range of x is a topical problem.

The focus of attention in performed theoretical and experimental studies of nonuniform In distribution in InGaN alloys has been investigation of phase separation. As a result, thermodynamic phase diagrams deter-

Growth parameters of epitaxial InGaN layers

Sample	T_s	Flux F_{Ga}, μm/h	Flux F_{In}, μm/h	High-frequency power, W	Nitrogen flux F_N, μm/h	Thickness of the buffer GaN layer grown by PA-MBE, μm	Thickness of the InGaN layer, nm
s196	630	0.13	0.43	130	0.36	0.2	70
s186	630	0.12	0.44	130	0.36	1.2	160
s187	630	0.12	0.44	130	0.36	1.2	60
s147	590	0.15	0.50	180	0.71	1.0	180

mining the regions of immiscibility in the InGaN layers depending on the growth temperature and stresses were constructed for the case of epitaxial growth on barrier or buffer layers [6–9]. It was found that the compression stresses emerging in the InGaN/GaN system lead to a substantial shift of the immiscibility region to larger x. In this case, it should be taken into account that the processes of stress relaxation in III–N compounds strongly differ from similar processes in other semiconductor compounds [10]. In addition, in some studies, a heavy influence of kinetic factors of the epitaxial growth on the development of the phase separation was shown. For example, Singh et al. [7] interpreted the limitation of the development of processes of phase separation to the extent of its complex suppression with lowering the substrate temperature (T_s) as the result of the accompanying large decrease in the surface mobility of the atoms of the growing layer.

For the growth of the InGaN layers and heterostructures on their base, the methods of vapor-phase epitaxy from organometallic (MOCVD) or chlorohydride compounds are often used. Molecular beam epitaxy (MBE) with the use of plasma activation of molecular nitrogen (PA-MBE) or high-temperature cracking of ammonia (NH_3-MBE) for obtainment of chemically active nitrogen has obtained somewhat less widespread application. It is noteworthy that considerably higher substrate temperatures $T_s > 750$°C are used for the growth of the InGaN layers with gas-phase technologies than for MBE ($T_s < 650$°C). Therefore, taking into account the kinetic growth features of the InGaN layers, this circumstance should lead to a substantial difference in the spatial In distribution in the layers grown by these technologies.

At present time, the best parameters of InGaN-based optoelectronic devices are attained with the use of MOCVD, and the highest values of x do not exceed 0.2. With respect to $In_xGa_{1-x}N$-based devices with a larger value of x and, correspondingly, with a longer wavelength, no technology has demonstrated satisfactory results. Therefore, it is impossible to unambiguously select the best technology for this composition region. It should be also noted that the best current results on the epitaxial growth of GaN are obtained with the use of the low-temperature PA-MBE [11].

In most studies devoted to the spatial In distribution in the InGaN layers, MOCVD-grown epitaxial layers have been investigated [12–14]. The studies using MBE are comparably few [15]. Moreover, in studies on the MBE growth of the InGaN layers, to our knowledge, relatively low $T_s < 590$°C have been used, while layers grown at higher temperatures have almost not been investigated, although, as we already showed in [16], the use of such conditions can lead to a substantial increase in intensity of the observed photoluminescence.

In this study, we investigated the main processes determining the spatial In distribution in the InGaN layers with various In contents ($x < 0.6$) grown by PA-MBE at 590–630°C. We specifically examined the interrelation between the spatial In distribution in the layers and their optical properties.

2. EXPERIMENTAL

The InGaN layers were grown (using a Compact 21T (Riber, France) PA-MBE installation) on c-Al_2O_3 substrates with a buffer GaN layer, as was previously described in detail [16]. The main growth parameters for the samples under study are listed in the table. To evaluate absolute fluxes of growth elements that arrive to the substrate, we used the values of maximum attainable growth rates of binary compounds GaN and InN at relatively low T_s, equal to 680 and 480°C, respectively. In this case, to determine the fluxes of Group III atoms, we used the data for growth processes carried out under nitrogen-enriched conditions, and to determine the flux of activated nitrogen those under metal-enriched conditions. The buffer GaN layers from 0.2 to 1.2 μm thick were grown using the same installation immediately prior to the growth of the InGaN layers at $T_s = 700$°C with the use of a stoichiometric ratio of the fluxes of Ga and activated nitrogen close to unity ($F_{Ga}/F_{N^*} \leq 1.1$), which provided a two-dimensional (2D) growth mechanism and a planar layer surface [17]. In the case of the growth of the sample s196 (see table), we used the so-called template (the c-sapphire substrate with the MOCVD GaN layer 3 μm thick). In the case of growth of the layer s147 on a standard buffer GaN layer (PA-MBE), an additional $In_xGa_{1-x}N$ metamorphic buffer layer 100 nm thick with a gradually increasing In content to $x = 0.6$ was grown.

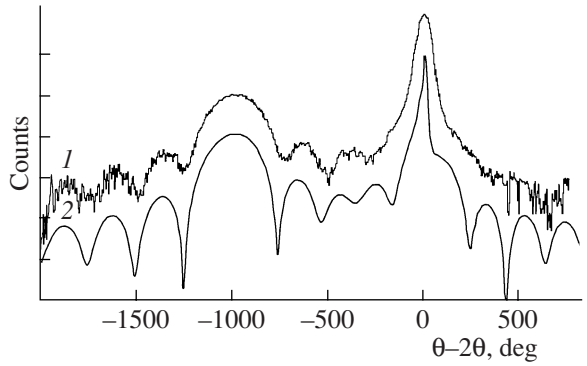

Fig. 1. θ–2θ XRDA rocking curves of the $In_xGa_{1-x}N$ layer with a thickness of 70 nm grown on the GaN template (s196): (*1*) experiment and (*2*) results of simulation under the assumption of pseudomorphic growth of the layer with $x = 0.10$ and a thickness of 70 nm.

For measurements of T_s, we used a Micron M680 infrared pyrometer, which allowed us to find that in the substrate center (we used quarters of the substrates of 50.7 mm in diameter), the value of T_s is 20–30°C lower than the values near the substrate edges. The growth and properties of the InGaN layers were characterized by the methods of reflection high-energy electron diffraction (RHEED) with a beam energy as high as 30 keV and laser interferometry at a wavelength of 660 nm. The use of this combination of methods in the context of a complex approach developed by us previously provides examination of the growth kinetic features of InGaN, including the direct determination of the growth rates of the InGaN epitaxial layers, their average composition, and efficiency of In incorporation [16]. To study the morphology and structure of the samples, we used scanning (SEM) and transmission (TEM) electron microscopy as well as atomic force microscopy (AFM). During the TEM measurements, we used selective angular diffraction. To determine x, we used local electron-probe microanalysis (EPMA) by the electron beam with an energy of 4 keV and a penetration depth into InGaN of about 50 nm [18]. The measurements of the spectra of microcathodoluminescence were carried out at electron energies as high as 5 keV with spatial resolution of ~1 μm. We also used X-ray diffraction analysis (XRDA) of rocking curves ω and θ–2θ of a symmetric reflection peak (0002) as well as the measurement of photoluminescence (PL) and PL excitation (PLE) spectra in a wide temperature range (25–300 K) with the use of a He–Cd laser with $\lambda = 325$ nm and power of 10 mW. To measure the PL spectra in the infrared (IR) range, we used an InGaAs laser diode with $\lambda = 809$ nm.

3. RESULTS AND DISCUSSION

3.1. $In_xGa_{1-x}N$ Layers with a Low Indium Content ($x \approx 0.1$)

The EPMA measurements of the In content at various points of the surface of sample s196 revealed the values $x = 0.08$–0.11, which virtually varied according to the gradient of T_s over the substrate; at characteristic distances of several micrometers, the spread of the values of x corresponded to the accuracy of its determination (±0.005). According to the XRDA data, the reflection (0002) was characterized by a symmetric shape of the θ–2θ curve with a full width at half maximum (FWHM) of 218″, and ω curve with the FWHM of 345″, which allows us to conclude that the layer has a high structural quality. Since the symmetric shape of the θ–2θ curve indicates an insignificant stress relaxation in the layer, the estimation of the In content by the location of the maximum of this curve was carried out under the assumption of pseudomorphic InGaN growth. According to this estimate, the value of $x = 0.10$ [19]. Figure 1 shows two θ–2θ curves, one of which with well-defined interference peaks was obtained experimentally; the second one was calculated for the layer with $x = 0.1$ and a thickness of 70 nm, irrespective of that one measured by TEM.

Studies of the morphology of layer s196 by SEM (Fig. 2a), AFM, and TEM showed that this sample has an atomically smooth surface with a mean-square deviation of ~1 monolayer in the limits of the field 200 × 200 nm and uniform image contrast of a transverse cleavage as shown in Fig. 2b. This pattern agrees with the observation of a line RHEED pattern throughout the growth time of layer s196. However, in certain points of the samples, we observed microdefects, pits ~1 μm in diameter, the density of which was low and amounted to ~10^7 cm^{-2}. Measurements of the cathodoluminescence characteristics in various points of the sample surface showed that these defects correspond to spectra having only a broad peak with an energy of ~2.2 eV (spectrum *1* in Fig. 3a). In regions with an atomically smooth surface, the characteristic cathodoluminescence spectra lie at higher energies and comprise the superposition of two bands peaked at energies of 3.12 and 2.90 eV, which substantially differ in spectral width (spectrum *2*). Figure 3b (curve *2*) shows the PL spectra of this sample, which lie in virtually the same spectral range. At $T = 25$ K, the high-energy peak with energy of 3.22 eV has a FWHM of ~50 meV, while the line peaked at 2.9 eV is wider by an order of magnitude. Contrast of the refractive index at the boundary between sapphire and the InGaN/GaN epitaxial structure leads to the emergence of the interference pattern of the long-wavelength part of the PL spectrum in the transparency region of the epitaxial film. To reveal the nature of both peaks, we measured the PLE spectrum with the detection energy in the region of the low-energy PL band, which is represented in Fig. 3b (curve *2*). The spectrum features a clearly pronounced absorption edge, the energy of which amounts to 3.28 eV at 25 K. An insignificant shift of the absorption edge to lower energies allows us to conclude that the layer is highly nonuniform in composition. In the energy region <3.2 eV, a noticeable density of states is absent. It fol-

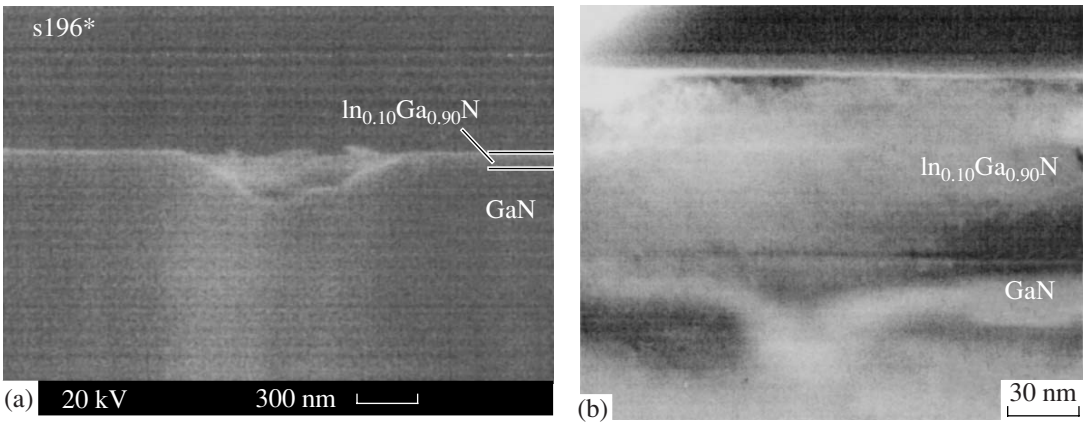

Fig. 2. Images of the cleavage of the $In_{0.1}Ga_{0.9}N$ layer with a thickness of 70 nm and $x = 0.10$ (s196) obtained by (a) SEM and (b) TEM for the reflection [0004]. A characteristic microdefect is represented in the SEM image.

lows from the presented data that a broad line in the cathodoluminescence and PL spectra peaked at 2.8–2.9 eV corresponds to radiative recombination with the participation of deep centers. A narrower peak (3.1–3.2 eV) can be apparently attributed to the edge luminescence shifted to lower energies with respect to the absorption edge (the Stokes shift of PL) by ~60–70 meV due to localization of carriers in the regions caused by a relatively slight nonuniformity of the layer by composition.

Therefore, the totality of structural and optical data indicate the absence of clear signs of phase segregation and stress relaxation in this $In_{0.1}Ga_{0.9}N$ layer (s196). This fact corresponds to theoretical phase diagrams of immiscibility of InGaN alloys with allowance made for compression stresses [8]. Notice that the absence of relaxation in this layer agrees with the value of critical thickness calculated by the People–Bean model, which exceeds 100 nm for the $In_{0.10}Ga_{0.90}N$ layer [20]. Continuous 2D growth observed during growth of this layer is in agreement with the experimental results of other authors with determination of critical thicknesses and compositions of bulk InGaN layers corresponding to the transition from the 2D to 3D growth, which were obtained during the layer growth by various technologies involving MOCVD [10], NH_3-MBE [21], and PA-MBE [22].

Despite the fact that the data represented above indicate a relatively high structural quality of this $In_{0.1}Ga_{0.9}N$ layer at a level up to several nanometers, its optical properties allow us to assume the presence of even lower scale nonuniformity of the layer by composition, probably caused by clustering of several In atoms according to the model suggested in [1].

3.2. $In_xGa_{1-x}N$ Layers with a Medium Indium Content ($x \approx 0.3$)

The use of this series of growth experiments of *c*-sapphire as the substrate confirmed our preliminary conclusion [16] about a higher efficiency of incorporation of In into the growing layer compared with layers grown at the same growth parameters but on templates. In this study, this conclusion is confirmed by EPMA measurements of x, which revealed an increase in x in layers s186 and s187 by a factor larger than 2 in comparison with sample s196. However, the value $x = 0.24$ determined by this method for these layers should be considered to be the lower estimate. This is caused by a block structure of the $In_xGa_{1-x}N$ layers with a characteristic block size of several hundreds of nanometers, which is illustrated in Fig. 4. The presence of block boundaries of several nanometers wide should substantially affect the detected signals of characteristic emission of Ga and In atoms, since a smaller film thickness within these boundaries determines deeper penetration of the electron beam into a buffer GaN layer. Consequently, with the presence of developed boundaries, an increase in the signal from Ga atoms should be observed, and the measured value $x = 0.24$ turns out smaller than the true one.

However, in [16], we used an in situ method of determination of the growth rate and average composition of the InGaN layers based on optical reflectometry, in which the signal was reflected from planar tops of blocks. In the case of the developed block structure of the layers, this leads to the use in calculations of a layer thickness somewhat overestimated compared with the value averaged over the layer surface with the allowance made for block boundaries and surface roughness, which is necessary for an precise estimation. As a result, the value of x turns out to be larger than the realistic one, and the value $x = 0.35$ obtained from these measurements should be considered as an upper estimate of the average indium content in the layers. Therefore, for these layers, we can accept the value $x = 0.30 \pm 0.05$, which indicates a three-fold increase in incorporation of indium compared with the MOCVD growth of the InGaN layers on the GaN template.

The studied layers s186 and s187 were grown at identical growth parameters and differed only in the

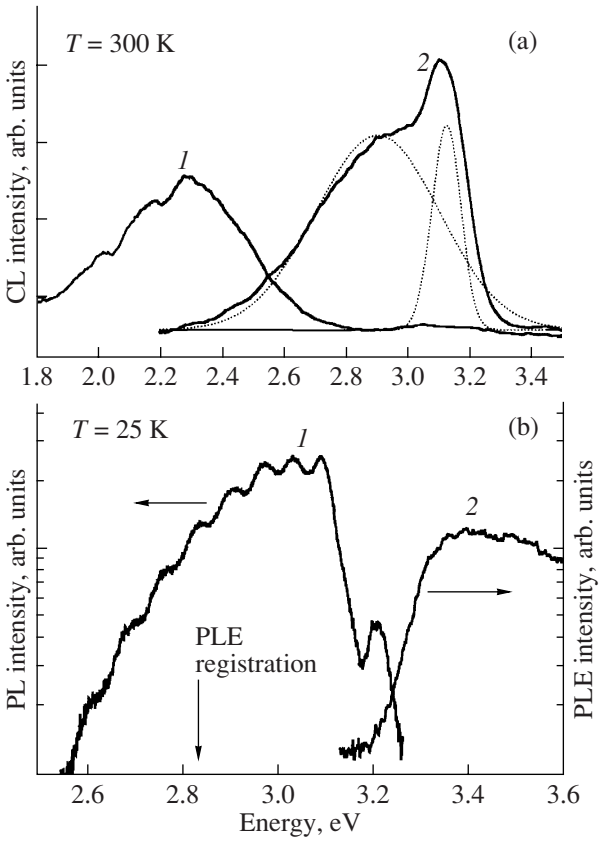

Fig. 3. (a) Cathodoluminescence spectra measured at various points of the surface of the $In_{0.1}Ga_{0.9}N$ layer (s196): (*1*) in the region of the microdefect and (*2*) at points of the surface with atomically smooth morphology (dotted lines represent the spectrum as superposition of two peaks in the Gaussian approximation). (b) Spectra of photoluminescence (*1*) and excitation of photoluminescence (*2*) of the $In_{0.1}Ga_{0.9}N$ layer (s196).

growth duration, which allowed us to study the effects associated with stress relaxation in the layers. TEM studies of the surface morphology showed that these layers have a block structure, which undergoes substantial variations during the growth. In both cases, for the first ~50 nm, we observed the growth of relatively large (as large as several hundreds of nanometers) blocks, on the tops of which the 2D growth mechanism with the atomically smooth surface is realized, which is indicated by the line RHEED pattern (Fig. 4a). This character of the surface was retained throughout the growth of a thin layer (s187), and in the beginning of the growth of a thick layer (s186). In the latter case, after the layer attained a thickness of 60–70 nm, for several minutes corresponding to the growth of a 5–10-nm layer, we observed the transition to a point RHEED pattern (Fig. 4b). After the growth of the thin layer was completed, the blocks had atomically smooth terrace-like tops with a characteristic lateral size of 500–1000 nm and interblock valleys as wide as 100 nm (Fig. 4c). The thick layer had a more developed 3D surface morphology and consisted of blocks with an average size of ≤100 nm (Fig. 4d).

Figure 5 shows the θ–2θ XRDA curves of these layers, which can be represented as a superposition of two peaks. The location of peak *1* in Fig. 5a in two approximations of an unrelaxed layer (pseudomorphic growth) and a completely relaxed layer gives $x = 0.29$ and 0.48, respectively. The relatively small FWHM of this peak allows us to estimate the thickness of this layer as 40 ± 5 nm under the assumption that $x = 0.29$. The location of peak *2* under the assumption of complete relaxation of the layer corresponds to indium content from $x = 0.20$ to 0.33 with a peak at $x = 0.27$. Unfortunately, the large width of this peak does not allow us to make estimates that are more precise. It is also noteworthy that the intensity of peak *1* for both layers (s186 and s187) is virtually identical, while the relative intensity of peak *2* in the thick layer s186 substantially increases compared with thin layer s187.

The above-mentioned data indicate a complex dependence of the layer morphology and phase segregation on the stress relaxation in the InGaN/GaN system, which proceeds in several stages. We can assume that in the beginning of the growth of the InGaN layers, only partial elastic strain relaxation proceeds through the formation of relatively large blocks with lateral sizes of hundreds of micrometers and an atomically smooth surface (s187). In these blocks, stresses are virtually retained until the layers attain a thickness of 60–70 nm, after which a pronounced plastic stress relaxation occurs in the blocks, which is also accompanied by a transition to a 3D growth mechanism with a characteristic size of the surface roughness at a level of several hundred nanometers (s186).

The profound effect of stress relaxation on the surface morphology of the InGaN layers can be caused by several factors. First, it is necessary to take into account the effect of stresses in the layer on its growth stoichiometry. According to thermodynamic concepts [23], elastic strains weaken the bond energy due to an increase in the Gibbs free energy by a value proportional to $(\Delta a/a)^2$, under the conditions of growth of the InGaN/GaN structure near the In–Ga liquidus. Therefore, this leads to an increase in the equilibrium nitrogen pressure above InGaN, in other words, increases the desorption of nitrogen. Stress relaxation "switches off" this additional reevaporation of nitrogen, and the incident nitrogen flux becomes excess. Therefore, we can assume realization of slightly III-enriched conditions during the pseudomorphic growth of a thin layer and initial ~50 nm of the thick layer, and transition to N-enriched conditions after the stress relaxation. Therefore, the transition from the line to point RHEED pattern observed by us (Fig. 4c) can be interpreted as caused by the change of metal-enriched growth conditions to N-enriched ones. In the case of PA-MBE of III–N compounds, such conditions lead to the growth of the layers with a planar or columnar morphology,

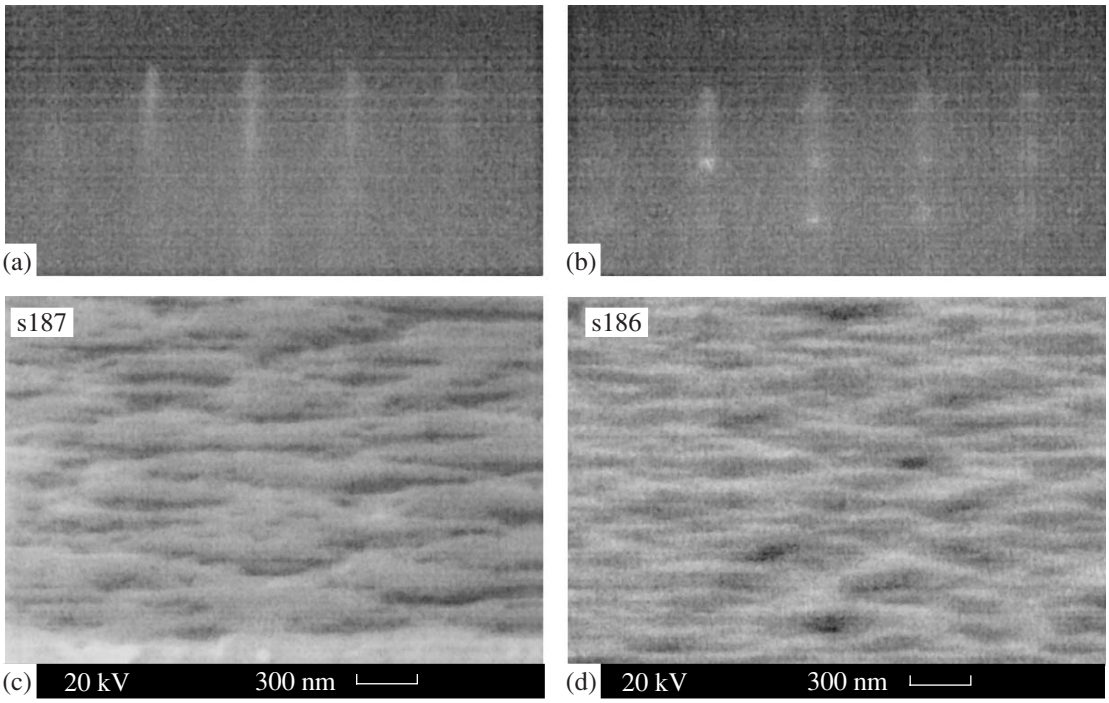

Fig. 4. RHEED patterns and SEM images (a, b and c, d, respectively) of the surface of the $In_{0.3}Ga_{0.7}N$ layers with the thickness equal to (a, c) 60 nm (sample s187) and (b, d) 160 nm (sample s186).

respectively [24]. In this sense, the surface morphology serves as an indicator of stress relaxation.

In addition, from the kinetic viewpoint, a more planar growth of stressed InGaN/GaN layers can be interpreted as caused by an increased surface mobility of adatoms due to a decrease in the height of energy barriers of surface diffusion in the case of compression stresses, as was theoretically described in [25].

The observed broadening of the XRDA peak for thick layer s186 compared with thin layer s187 indicates both an increase in the degree of imperfection of the layers during growth and an increase in nonuniformity of the In distribution, i.e., on the formation of the InGaN clusters with various compositions. As the causes of cluster formation in layer s186, first of all, phase segregation should be considered, the possibility of which follows from the thermodynamic instability of the $In_xGa_{1-x}N$ alloy with $x \approx 0.3$ under the conditions where compression elastic stresses that limit the development of phase segregation decrease due to relaxation. However, for this layer, it is impossible to suggest a pronounced development of phase segregation, since the characteristic peak is absent in the θ–2θ XRDA curve in the region of binary InN compound, the final point of phase segregation. This is probably caused by kinetic limitations of attainment the thermodynamically stable InGaN phases by the decomposing solution because of relatively low growth temperatures (T_s = 630°C). Therefore, in this case, we deal with the initial or weak development of phase segregation, which is accompanied by only a slight increase in the composition nonuniformity in the growing InGaN layer.

Investigations of optical properties of the layers with various thicknesses revealed substantial differences in the shape and intensity of the PL and cathodoluminescence spectra of these layers in the spectral region of 1.9–2.6 eV (480–650 nm). First, as it is shown in Fig. 6a, while only the main peak (spectrum *1*) at 2.16 eV is observed in the PL spectrum of thin layer s187, the thick layer has several peaks with energies of 1.96, 2.24, and 2.42 eV (spectrum *2*). This fact confirms the conclusions made on the basis of the XRDA data and concerned with a more uniform distribution of indium in this layer. We can assume that these peaks correspond to the InGaN clusters with various relative In contents with respect to a surrounding matrix and size. Second, the thick layer is characterized by an intensity of integrated PL higher than the thin layer by more than an order of magnitude. In our opinion, this fact can be due to effective localization of carriers in coherent In-enriched InGaN clusters, the formation of which is additionally stimulated by 3D growth under the N-enriched conditions.

3.3. $In_xGa_{1-x}N$ Layers with a High Indium Content ($x \approx 0.6$)

For the growth of the layer with the highest In content for this series (s147), we used the relatively low T_s = 590°C (see table), which should lead to an increase in incorporation of indium into the growing layer [16].

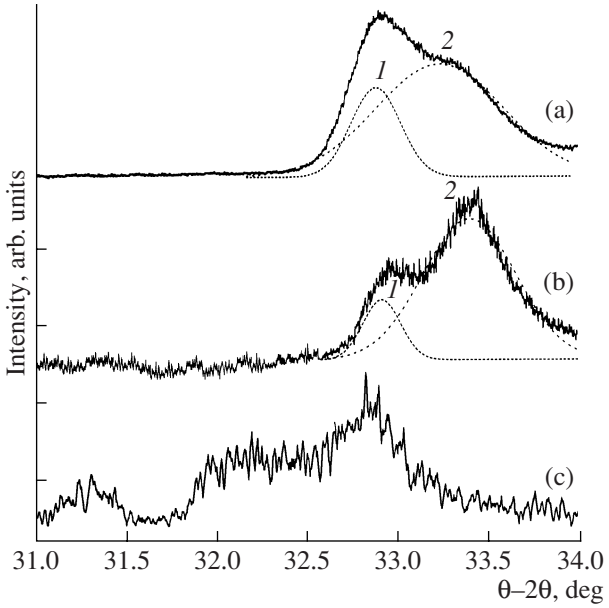

Fig. 5. θ–2θ XRDA rocking curves for various $In_xGa_{1-x}N$ layers: (a) $x = 0.3$, thickness of 60 nm (s187); (b) $x = 0.3$, thickness of 160 nm (s186); and (c) $x = 0.6$, thickness of 180 nm (s147). Dotted lines represent the curves as superposition of two peaks (*1* and *2*) in the Gaussian approximation.

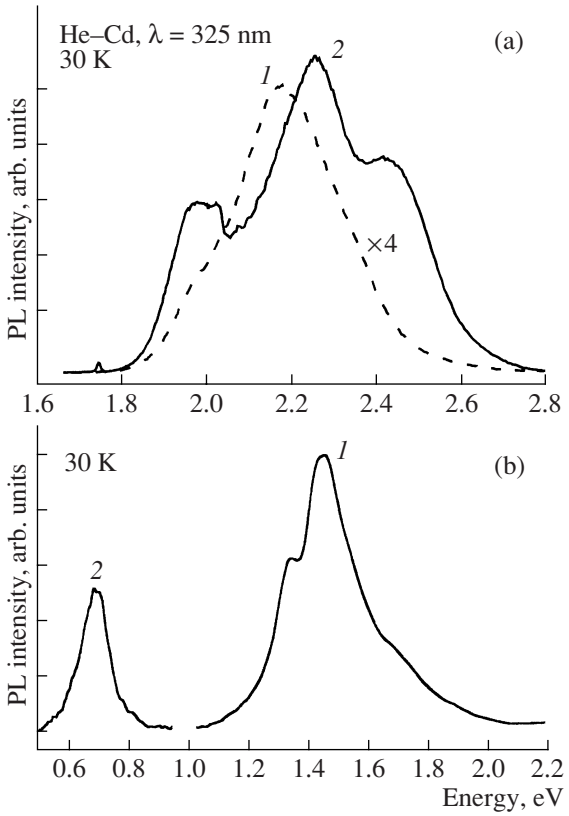

Fig. 6. (a) Low-temperature (30 K) photoluminescence spectra of the $In_{0.3}Ga_{0.7}N$ layers grown under identical conditions and with thicknesses of (*1*) 60 nm (s187) and (*2*) 160 nm (s187). (b) Photoluminescence spectra of the $In_{0.6}Ga_{0.4}N$ layer (s147) measured under excitation using (*1*) a He–Cd laser or (*2*) an InGaAs laser.

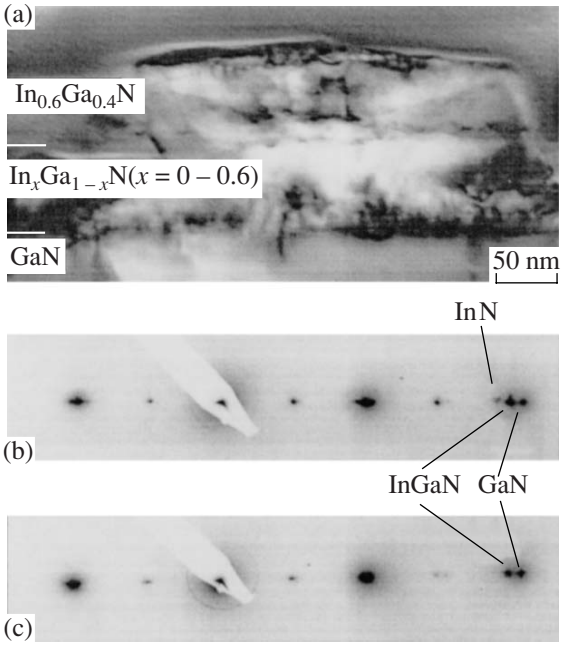

Fig. 7. (a) TEM image for reflection [0004] of the $In_{0.6}Ga_{0.4}N/In_xGa_{1-x}N(x = 0–0.6)/GaN$ structure (s147) and the patterns of selective angular diffraction measured (b) for the main $In_{0.6}Ga_{0.4}N$ layer and (c) for the buffer metamorphic layer.

Indeed, the In content in this layer determined using laser interferometry was $x = 0.6 \pm 0.1$. The same value of x was determined by EPMA. Studies of the layer morphology showed that this layer, similarly to above-described layers, had a block structure with an average block size of 100–200 nm, and the blocks had relatively flat tops. In addition, using the probe methods, we revealed large-scale (3–4 μm) nonuniformities in the indium distribution over the layer surface. In these regions, enrichment with In was observed.

Figure 5c represents the θ–2θ XRDA curve of this layer, which indicates the existence of various InGaN phases including a broad band in the region of medium compositions $x = 0.45–0.65$ (estimation under the assumption of complete relaxation) and a solid solution in the region of binary InN. The last observation directly indicates a pronounced development of phase separation. This phenomenon was confirmed by the TEM data, which not only revealed highly developed contrast corresponding to various cluster formations $In_xGa_{1-x}N$ (Fig. 7a) in images of transverse cleavages of the samples, but also revealed additional reflections characteristic of the InN phase in the pattern of selective angular diffraction (Figs. 7b, 7c) [22].

Finally, measurements of PL spectra of this layer (Fig. 6b) revealed the presence of two peaks *1* and *2* belonging to different spectral regions in each measurement point. The second peak manifests itself in the infrared region with λ = 1700–1800 nm, and the first peak manifests itself near the spectral edge of visible

light λ = 700–900 nm. Since peak *2* is usually observed in the PL spectra of the binary compound InN, its manifestation can be considered as additional evidence of the fact that phase separation in the layer is close to completeness. However, the intensity of both peaks is substantially lower than the intensity of PL peaks observed for the layers with low and medium In content.

4. CONCLUSIONS

As a result of the performed studies, we established features of formation of the spatially nonuniform distribution of indium in the $In_xGa_{1-x}N$ layers with various In contents (x = 0.1–0.6) grown by PA-MBE at relatively low growth temperatures (590–630°C).

It is established that, at a low In content ($x \approx 0.1$), the layers grow pseudomorphically at least to a thickness of 70 nm, and these layers are characterized by a highly uniform morphology at the nanolevel and microlevel, which confirms their thermodynamic stability. In this case, the measurements of the PL and cathodoluminescence spectra of the layers are indicative of the formation of localized states near the band gap edge and formation of deep defect levels with a substantially lower concentration.

In the layers with the medium value $x \approx 0.3$, we observed signs of a nonuniform In distribution, which is associated with the stress relaxation and onset of the phase separation. It is found that relaxation of the layers proceeds in several stages with the formation of the block structure with blocks having a lateral size of 1000 nm and an atomically smooth surface in the beginning of the growth. After attainment of a layer thickness of 50–70 nm, the transition from the planar to three-dimensional surface of the tops of the blocks and a decrease in the characteristic size of the blocks are observed. We attribute this phenomenon to the variation in the growth stoichiometry from III-enriched to N-enriched due to an abrupt decrease in reevaporation of nitrogen from InGaN after relaxation of compression elastic stresses. In addition, the observed planar surface in the beginning of the growth can be attributed to the compression character of stresses in the InGaN/GaN system, which leads to an increase in the surface mobility of adatoms. It is shown that layers with more uniform In distribution exhibit more intense PL at energies of 2.0–2.2 eV. However, the absence of signs of formation of the phase with a composition close to binary InN in these layers indicates that phase separation is incomplete. Because of low growth temperatures, this fact is apparently determined by the effect of kinetic limitations to the development of this process.

For the layers with a large value $x \approx 0.6$, it is possible to affirm the almost complete phase separation, including formation of a phase with composition close to InN, which was confirmed by the observation of two peaks both in the XRDA pattern (one peak in the region of binary InN) and in the PL spectrum (one peak is arranged near the edge of the visible spectral range λ = 700–900 nm, and the second peak is arranged in the infrared region with λ = 1700–1800 nm).

ACKNOWLEDGMENTS

This study was supported by the Russian Foundation for Basic Research (project nos. 05-02-16934, 06-02-17306, and 07-02-12233-ofi) and by the Program of Basic Research of the Presidium of the Russian Academy of Sciences "Quantum Nanostructures."

REFERENCES

1. S. F. Chichibu, A. Uedono, T. Onuma, et al., Nature Mater. **5**, 810 (2006).
2. C. Wetzel and T. Detchprohm, MRS Int. J. Nitride Semicond. Res. **10**, 2 (2005).
3. M. Yamada, Y. Narukawa, and T. Mukai, Jpn. J. Appl. Phys. **41**, L246 (2002).
4. A. Kikuchi, M. Tada, K. Miwa, and K. Kishino, Jpn. J. Appl. Phys. **43**, L1524 (2004).
5. O. H. Ham, K. H. Ha, S. N. Lee, et al., in *Proceedings of the International Workshop on Nitride Semiconductors, Kyoto, Japan, 2006*, p. 70.
6. I. Ho and G. B. Stringfellow, Appl. Phys. Lett. **69**, 2701 (1996).
7. R. Singh, D. Doppalapudi, T. D. Moustakas, and L. T. Romano, Appl. Phys. Lett. **70**, 1089 (1997).
8. S. Y. Karpov, MRS Int. J. Nitride Semicond. Res. **3**, 16 (1998).
9. M. Rao, D. Kim, and S. Mahajan, Appl. Phys. Lett. **85**, 1961 (2004).
10. C. A. Parker, J. C. Roberts, S. M. Bedair, et al., Appl. Phys. Lett. **75**, 2776 (1999).
11. X. Wang, S. B. Che, Y. Ishitani, and A. Yoshikawa, J. Appl. Phys. **99**, 073512 (2006).
12. Y. T. Moon, D. J. Kim, J. S. Park, et al., Appl. Phys. Lett. **79**, 599 (2001).
13. S. Pereira, M. R. Coreia, E. Pereira, et al., Appl. Phys. Lett. **80**, 3913 (2002).
14. S. W. Feng, T. Y. Tang, Y. C. Lu, et al., J. Appl. Phys. **95**, 5388 (2004).
15. F. B. Naranjo, M. A. Sanchez-Garcia, F. Calle, et al., Appl. Phys. Lett. **80**, 231 (2002).
16. S. V. Ivanov, V. N. Jmerik, T. V. Shubina, et al., J. Cryst. Growth **301**, 465 (2007).
17. V. N. Jmerik, A. M. Mizerov, T. V. Shubina, et al., Pis'ma Zh. Tekh. Fiz. **33** (8), 36 (2007) [Tech. Phys. Lett. **33**, 333 (2007)].
18. Ya. V. Domracheva, L. A. Bakaleinikov, E. Yu. Flegontova, et al., in *Proceedings of the EMAS 2007, 10th European Workshop on Modern Developments and Applications in Microbeam Analysis, Antwerp, Belgium, 2007*.
19. K. P. O'Donnell, J. F. W. Mosselmans, R. W. Martin, et al., J. Phys.: Condens. Matter. **13**, 6977 (2001).
20. R. People and J. C. Bean, Appl. Phys. Lett. **47**, 322 (1985).
21. N. Grandjean, B. Damilano, and J. Massies, J. Phys.: Condens. Matter. **13**, 6945 (2001).
22. C. Adelmann, J. Simon, G. Feuillet, et al., Appl. Phys. Lett. **76**, 1570 (2000).
23. S. V. Ivanov, P. D. Altukhov, T. S. Argunova, et al., Semicond. Sci. Technol. **8**, 347 (1993).
24. J. Neugebauer, T. Zywietz, and M. Scheffler, J. Northrup. Appl. Surf. Sci. **159–160**, 355 (2000).
25. M. Shroeder and D. E. Wolf, Surf. Sci. **375**, 129 (1997).

Translated by N. Korovin